GENES, CHROMOSOMES & CANCER 52:873–886 (2013)

RESEARCH ARTICLES

Comprehensive Genetic Analysis Identifies a Pathognomonic *NAB2/STAT6* Fusion Gene, Nonrandom Secondary Genomic Imbalances, and a Characteristic Gene Expression Profile in Solitary Fibrous Tumor

Arezoo Mohajeri,[1] Johnbosco Tayebwa,[1] Anna Collin,[1] Jenny Nilsson,[1] Linda Magnusson,[1] Fredrik Vult von Steyern,[2] Otte Brosjö,[3] Henryk A. Domanski,[4] Olle Larsson,[5] Raf Sciot,[6] Maria Debiec-Rychter,[7] Jason L. Hornick,[8] Nils Mandahl,[1] Karolin H. Nord,[1] and Fredrik Mertens[1]*

[1]Department of Clinical Genetics, University and Regional Laboratories, Lund University, Lund, Sweden
[2]Department of Orthopedics, Skåne University Hospital, Lund University, Lund, Sweden
[3]Department of Orthopedics, Karolinska University Hospital, Solna, Sweden
[4]Department of Pathology, University and Regional Laboratories, Lund University, Lund, Sweden
[5]Department of Pathology, Karolinska University Hospital, Solna, Sweden
[6]Department of Pathology, KU Leuven and University Hospitals, Leuven, Belgium
[7]Center for Human Genetics, KU Leuven and University Hospitals, Leuven, Belgium
[8]Department of Pathology, Brigham and Women's Hospital, Harvard Medical School, Boston, USA

Solitary fibrous tumor (SFT) is a mesenchymal neoplasm displaying variable morphologic and clinical features. To identify pathogenetically important genetic rearrangements, 44 SFTs were analyzed using a variety of techniques. Chromosome banding and fluorescence in situ hybridization (FISH) showed recurrent breakpoints in 12q13, clustering near the *NAB2* and *STAT6* genes, and single nucleotide polymorphism array analysis disclosed frequent deletions affecting *STAT6*. Quantitative real-time PCR revealed high expression levels of the 5'-end of *NAB2* and the 3'-end of *STAT6*, which at deep sequencing of enriched DNA corresponded to *NAB2/STAT6* fusions. Subsequent reverse-transcriptase PCR (RT-PCR) analysis identified a *NAB2/STAT6* fusion in 37/41 cases, confirming that this fusion gene underlies the pathogenesis of SFT. The hypothesis that the *NAB2/STAT6* fusions will result in altered properties of the transcriptional co-repressor NAB2 - a key regulator of the early growth response 1 (EGR1) transcription factor – was corroborated by global gene expression analysis; SFTs showed deregulated expression of EGR1 target genes, as well as of other, developmentally important genes. We also identified several nonrandom secondary changes, notably loss of material from 13q and 14q. As neither chromosome banding nor FISH analysis identify more than a minor fraction of the fusion-positive cases, and because multiple primer combinations are required to identify all possible fusion transcripts by RT-PCR, alternative diagnostic markers might instead be found among deregulated genes identified at global gene expression analysis. Indeed, using immunohistochemistry on tissue microarrays, the top up-regulated gene, *GRIA2*, was found to be differentially expressed also at the protein level.

INTRODUCTION

Solitary fibrous tumor (SFT) is a mesenchymal tumor composed of fibroblast-like neoplastic cells arranged in a patternless way in a collagenous matrix. Several, often overlapping, morphologic patterns have been described, and tumors showing more prominent branching vessels were previously known as hemangiopericytomas, while those with a significant adipocytic admixture were called lipomatous hemangiopericytomas. As all morphologic subtypes share certain cellular features as well as immunophenotypic characteristics, such as frequent expression of CD34, they are now considered a

Additional Supporting Information may be found in the online version of this article.

Arezoo Mohajeri and Johnbosco Tayebwa contributed equally to this work.

Supported by: The Swedish Cancer Foundation; the National Research Council of Sweden; the Gunnar Nilsson Cancer Foundation; the IngaBritt and Arne Lundberg Foundation; the Swedish Childhood Cancer Foundation; and the Medical Faculty of Lund University

*Correspondence to: Fredrik Mertens, Department of Clinical Genetics, University Hospital, SE-221 85 Lund, Sweden.
E-mail: fredrik.mertens@med.lu.se

Received 14 May 2013; Accepted 16 May 2013

DOI 10.1002/gcc.22083

Published online 12 June 2013 in Wiley Online Library (wileyonlinelibrary.com).

single biologic entity (Vallat-Decouvelaere et al., 1998; Guillou et al., 2002; Weiss and Goldblum, 2008). Since the first description of SFT as a pleural neoplasm (Klemperer and Rabin, 1931), it has become clear that it can occur virtually anywhere in the body. Irrespective of anatomical site, it typically presents as a painless lump in middle-aged adults, without any gender predilection. There are currently no specific markers to confirm the diagnosis of SFT. Furthermore, some 10% of cases behave aggressively, with local recurrences and/or distant metastases; tumor site, size, growth pattern, and mitotic activity are associated with aggressive behavior, but prediction of outcome is difficult in the individual case (Fletcher et al., 2013a). SFTs are in general insensitive to chemo- and radiotherapy, and, hence, surgery with adequate margins is a prerequisite for cure (Demicco et al., 2012).

Because of the differential diagnostic problems, the difficulties in predicting outcome in SFT patients, and the lack of treatment targets in malignant cases, efforts have been made to identify characteristic genetic markers. While chromosome banding, comparative genomic hybridization and array-based genomic analyses have failed to identify any consistent aberrations (Miettinen et al., 1997; Bertucci et al., 2013; Mitelman Database of Chromosome Aberrations and Gene Fusions in Cancer, 2013), next generation sequencing (NGS) of RNA and DNA from SFTs recently resulted in the identification of a *NAB2/STAT6* fusion gene in the majority, if not all, cases (Chmielecki et al., 2013; Robinson et al., 2013).

In this study, we employed a variety of investigative approaches—high-resolution single nucleotide polymorphism (SNP) arrays, NGS, global gene expression analysis, chromosome banding, quantitative real-time PCR (qRT-PCR), reverse-transcriptase PCR (RT-PCR), fluorescence in situ hybridization (FISH), and immunohistochemistry (IHC)—on a series of SFTs, disclosing a high frequency of *NAB2/STAT6* fusions, nonrandom secondary chromosomal changes, as well as gene and protein expression data of potential diagnostic relevance.

MATERIALS AND METHODS

Patients and Tumors

The study included tumors diagnosed as SFT from 44 patients (24 women, 20 men; median age at diagnosis 53 years, range 16–89 years). Clinical features are shown in Supporting Information Table S1. In summary, 21 tumors were located in the extremities, followed by pleura/thoracic cavity ($n = 9$), trunk wall ($n = 5$), retroperitoneum/abdominal cavity ($n = 3$), head and neck ($n = 3$), and meninges/spinal cord ($n = 3$). Fresh tumor samples were obtained for cytogenetic and molecular analyses from the sarcoma centres in Lund and Stockholm, Sweden, and Leuven, Belgium. The histopathologic diagnoses were based on the criteria outlined by Guillou et al. (2002). The sampling, storage and analysis of the tumors and blood samples included in this study were approved by the Regional Ethics Committee of Lund University.

Cytogenetic and FISH Analyses

Cell culturing, harvesting, and G-banding were performed as described and the karyotypes were written following the recommendations of the International System for Human Cytogenetic Nomenclature (Mandahl et al., 1988; Shaffer et al., 2009).

The bacterial artificial chromosome (BAC) and fosmid probes that were used to delineate the breakpoints in 12q13 were obtained from the BACPAC Resource Center (http:/bacpac.chori.org). The probes are specified in Supporting Information Table S2. Clone preparation, hybridization and analysis were performed as described (Jin et al., 2012).

SNP Array Analysis

DNA from 20 patients with SFT was analyzed with SNP array to detect global copy number changes and allelic imbalances. From two patients, two tumor samples were available, and from six of the patients also a blood sample was analyzed (data not shown). The DNA was extracted from fresh frozen tumor biopsies using the DNeasy Tissue Kit including the optional RNase A treatment, according to the manufacturer's instructions (Qiagen, Valencia, CA). DNA concentrations were measured with a Nanodrop ND-1000 spectrophotometer (Saveen & Werner AB, Malmö, Sweden). DNA was hybridized to the Illumina Human Omni-Quad version 1.0 BeadChips (Illumina, San Diego, CA), containing 1.2 million markers, following standard protocols supplied by the manufacturer. The positions of SNPs were according to the UCSC hg 19/NCBI Build 37. SNP data analysis was performed using the BeadStudio software version 3.1 (Illumina), and imbalances were identified through visual inspection.

Constitutional copy number variations were excluded through comparison with the Database of Genomic Variants, (http://projects.tcag.ca/variation/; accessed September 12, 2012). Nonrecurrent aberrations smaller than 0.5 Mb were also excluded from the aberration list.

Global Gene Expression Analysis

From a previous study (Möller et al., 2011), global gene expression data were available for five SFTs and 35 other soft tissue tumors (17 low-grade fibromyxoid sarcomas LGFMS, six desmoid tumors, six extraskeletal myxoid chondrosarcomas, and six myxofibrosarcomas) serving as controls (accessible at NCBI's Gene Expression Omnibus database: http://www.ncbi.nlm.nih.gov/geo/query/acc.cgi?acc=GSE24369). Extraction of total RNA from frozen tumor biopsies, RNA concentration and quality measurements and hybridization of cDNA to the Human GeneChip® Gene 1.0 ST array (Affymetrix, Santa Clara, USA) were performed as described (Möller et al., 2011). Background correction, normalization and probe summarization were done using the Robust Multi-chip Average (RMA) method implemented in the Expression Console software version (v) 1.0 (Affymetrix).

qRT-PCR Analysis

To detect any differences in the expression levels consistent with breakage within *NAB2* or *STAT6*, TaqMan gene expression assays were performed on 35 SFTs using probes mapping to the 5'- and 3'-ends of each gene. RNA from desmoid tumors, low-grade fibromyxoid sarcomas, synovial sarcomas, and myxofibrosarcomas were used as control. *HPRT1* was used as endogenous control, based on its stable expression at global gene expression analysis. The following TaqMan gene expression assays were used: Hs01082003_m1 (*NAB2* 5'; exons 1–2), Hs00195573_m1 (*NAB2* 3'; exons 6–7), Hs01127471_g1 (*STAT6* 5'; exons 5–6), Hs00598625_m1 (*STAT6* 3'; exons 19–20), and Hs02800695_m1 (*HPRT1*). Total RNA from one of the desmoid tumors was used as calibrator in both series. qRT-PCR was performed according to the manufacturer's instructions and all reactions were run in triplicate (Applied Biosystems, Foster City, CA). Calculations were done using the comparative C_T method (i.e., $\Delta\Delta C_T$ method) (Livak and Schmittgen, 2001), using the SDS software 1.3.1.

Capturing, Sequencing, and Analysis of Target Genomic Region

In order to identify the genomic breakpoints involved in potential fusion events, DNA was extracted from 11 SFT samples and four blood samples from 10 patients. Baits for enrichment of a 1.0 Mb region in chromosome band 12q13 (Chr12: 57,300,000–58,300,000) were obtained from Agilent Technologies (Stockholm, Sweden) and the target region was captured using solution-based targeted enrichment by hybridization (Agilent SureSelect XT Custom MP3). Window Masker and Repeat Masker were used to exclude repeated sequences, leaving 67.5% of the nucleotides in the target region available for capture. Tumor and blood DNA (3 μg of input material) was fragmented to 300 bp using a Covaris S2 instrument. At SciLifeLab (Stockholm, Sweden), clustering was performed on a cBot cluster generation system using a HiSeq paired-end read cluster generation kit according to the manufacturer's instructions. The samples were sequenced on an Illumina HiSeq 2000 and base conversion was done using Illumina's OLB v1.9, according to the manufacturer's instructions. The generated raw sequence files contained paired-end reads (read-length 101 bp) in fastq format with base quality scores in the phred64/Illumina 1.3+ format.

For each library (sample), the paired-end reads were mapped to the human genome reference sequence (UCSC hg19) using the functions "index," "aln," and "sampe" of the BWA program (Li and Durbin, 2009). The results of the alignment were stored in the Binary Alignment/Map (BAM) format using the SAMtools package (Li et al., 2009). Addition of readgroups, coordinate sorting of readpairs, removal of duplicate reads, building the bam index and validation of the bam files were done using the Picard toolkit (http://picard.sourceforge.net/, accessed Jan 10, 2013). Local realignment around indels for tumor and normal pairs, and base quality score recalibration were done using the IndelRealigner and BaseRecalibrator, respectively, from the Broad Institute Genome Analysis Toolkit (De Pristo et al., 2011).

FusionMap was employed to identify gene fusions (Ge et al., 2011), either using unmapped reads extracted from the BAM files or using the raw reads in fastq files. Methods for general structural variant detection such as Pindel v0.2.4t (Ye et al., 2009) and DELLY v0.0.9 (Rausch et al., 2012) were also used in order to delineate the structural rearrangements resulting in gene

fusions. Pindel does not detect interchromosomal rearrangements and performs best in detection of structural variants less than 10 kbp, whereas DELLY is able to detect interchromosomal rearrangements and structural variants larger than 10 kbp (Rausch et al., 2012).

RT-PCR

Total RNA was extracted from frozen tumor samples using the Qiazol reagent (Qiagen, Valencia, CA). Reverse transcription and PCR amplifications were performed as described (Panagopoulos et al., 2001; Jin et al., 2012). Primers specific for *NAB2* and *STAT6* were designed to detect possible fusion transcripts (Supporting Information Table S3). Transcripts were amplified using an initial denaturation for 2 min at 94°C, followed by 30 cycles of 30 sec at 94°C, 30 sec at 58°C, and 3 min at 72°C and a final extension for 3 min at 72°C. Amplified fragments were purified from agarose gels and directly sequenced using the Big Dye v1.1 cycle sequencing kit (Applied Biosystems, Foster City, USA) on an ABI-3130 genetic analyzer (Applied Biosystems). The BLASTN software (http://www.ncbi.nlm.nih.gov/blast) was used for the analysis of *NAB2* and *STAT6* sequence data.

IHC

A tissue microarray (TMA), previously described in detail by Möller et al. (2011), with nine SFTs, 10 low-grade fibromyxoid sarcomas, 11 myxofibrosarcomas, 12 desmoid tumors, six extraskeletal myxoid chondrosarcomas, and one myoepithelial tumor was used to evaluate the expression of GRIA2. Each case was represented twice per TMA block, and the TMA blocks were prepared in duplicate; thus, four cores per case were studied. Epitope retrieval was achieved by heating 4 μm TMA slides in citrate buffer (pH 6.0) in a pressure cooker. The sections were stained with an anti-GRIA2 rabbit monoclonal antibody (clone EP929Y; Abcam, Cambridge, MA) at 1:100 dilution. The Evision Plus detection system (Dako, Carpinteria, CA) was used as a secondary antibody.

Statistical Analyses

Correlation-based principal component analysis and hierarchical clustering analysis of global gene expression data were performed using the Qlucore Omics Explorer version 2.2 (Qlucore, Lund, Sweden). Differences between tumor groups in $\log_2$ transformed expression data were calculated using a *t*-test and corrections for multiple testing were based on the Benjamini-Hochberg method (Qlucore). Genes with a P-value < 0.001 and a false discovery rate < 0.01 were considered significantly altered.

For genes implicated in EGR1-signaling, the Chi Square test, two-tailed, with Yates' correction was used when comparing proportions of deregulated genes.

RESULTS

Cytogenetic and FISH Findings

A total of 47 samples from 44 SFT patients were analyzed after short-term culturing, revealing an abnormal karyotype in 31 samples from 29 patients (Table 1). Considering only one sample per patient, 13 had pseudodiploid, five hypodiploid, five hyperdiploid, two near-triploid, and four near-tetraploid chromosome numbers. The most common breakpoint in structural rearrangements was 12q13 (five cases). The most frequent imbalances, combining unbalanced structural and numerical changes, were loss of 13q14-q32 (five cases), and, in three cases each, loss of 1q31-q43, 7p22, 12q13, and 14q22-qter and gain of chromosome 8. No recurrent interchromosomal rearrangement was seen.

Metaphase and interphase FISH analysis of 14 cases revealed at least one breakpoint in the ~1 Mb region flanked by RP11–976L20 and RP11–571M6, i.e., near or within the *NAB2* and *STAT6* genes, in nine cases (Table 1).

SNP Array Results

SNP array analysis was performed on 22 samples from 20 patients with SFT (Table 1, Supporting Information Table S4). Imbalances (ranging from 1 to >25 per sample) were found in 15 of the patients, the most common being a hemizygous deletion in 12q13 (six patients, with minimal shared regions at 57.515-57.521 Mb and 57.527-57.615 MB in five patients each; Supporting Information Table S5). In addition, three patients showed complex rearrangements with multiple gained regions in 12q. Other imbalances seen in three or four cases included hemizygous deletions affecting 10q (including homozygous deletion in one patient), 13q and 14q, and gain of 5p, 8p (including amplification in one patient) and 8q.

TABLE 1. Summary of Genetic Findings in 44 Solitary Fibrous Tumors

Case no.	Karyotype	FISH[a]	SNP[b]	qRT-PCR[c]	GGE[d]	NGS[e]	IHC[f]	RT-PCR/PCR[g]
1A.	46,XY,inv(12)(q14q24)	ND	Del 12q	ND	ND	*NAB2* In6/	ND	ND/*TERT*-
1B.	46,XY,inv(12)(q14q24)/47,idem,+5	ND	Del 12q	*NAB2* 5' *STAT6* 3'	ND	*STAT6* Ex17 *NAB2* In6/ *STAT6* Ex17	ND	Ex6-Ex18/ND
2.	46,XY,t(6;12;19)(p22;q13;p13)	ND	Del 12q	*NAB2* 5' *STAT6* 3'	Yes	*NAB2* In6/ *STAT6* In16, *R3HDM2* Ex6/ *STAT6* Ex17, *TRAPPC5* In1/ *STAT6* In13	Pos	Ex6-Ex18/ *TERT*-
3.	45,XX,-14	ND	Del 12q, −14	*STAT6* 3'	ND	ND	ND	Ex2-Ex6/ *TERT*-
4A.	72,XX,-X,del(1)(q21),add(7)(p22),inc	ND	ND	ND	ND	ND	ND	ND/ND
4B.	Failure	ND	ND	ND	ND	ND	Pos	Ex6-Ex18/ND
5.	77,XXY,+Y,+3,+8,+10,+12,+14,+17, +21/78,idem,+19	ND	ND	ND	ND	ND	ND	ND/ND
6.	46,XY,t(2;17)(p16;q11),ins(7;11) (q36;q14q23)	ND	ND	*NAB2* 5'	ND	ND	ND	Ex2*-Ex1b*/ ND
7.	47,XX,+5	Negative	ND	*NAB2* 5'	ND	ND	ND	Ex6-Ex17/ND
8.	41,XX,-3,-4,-5,-9,-10,-12,-13,-17,+20, +2mar	ND	Complex gain/loss 12q, −13	Negative	ND	ND	ND	Ex4-Ex3/ND
9.	46,XY	ND	Normal	Negative	ND	ND	ND	Neg/ND
10.	46,XX	ND	Del 14q	ND	ND	ND	ND	Ex5-Ex18/ *TERT*-
11.	45,XX,tas(14;19)(p13;q13)	ND	Del 13q	Negative	ND	*NAB2* Ex2/ *STAT6* Ex3	Pos	Ex2*-Ex3*/ *TERT*-
12.	46,XY	Negative	Normal	Negative	ND	ND	ND	Ex2-Ex6/ND
13.	46,XY	ND	Abnormal	Negative	ND	ND	ND	Ex4-Ex3/ND
14.	46,XX	ND	ND	*NAB2* 5'	ND	ND	ND	Ex4-Ex5/ND
15.	45,XX,-13	ND	ND	*NAB2* 5'	ND	ND	ND	Ex6-Ex17/ND
16.	46,XX	ND	ND	ND	ND	ND	ND	Ex5-Ex18/ND
17.	48,XX,+6,+?del(14)(q22)	Negative	Abnormal	*NAB2* 5' *STAT6* 3'	Yes	*NAB2* In6/ *STAT6* Ex16	Neg	Ex6-Ex17/ *TERT*+ C228T
18.	46,XY	ND	Normal	*NAB2* 5'	ND	ND	ND	Ex7-Ex3/ *TERT*-
19.	46,XX	ND	Normal	ND	ND	*NAB2* In6/ *STAT6* In15	ND	Ex6-Ex17/ *TERT*-

TABLE 1. (Continued)

Case no.	Karyotype	FISH[a]	SNP[b]	qRT-PCR[c]	GGE[d]	NGS[e]	IHC[f]	RT-PCR/PCR[g]
20.	46,XX,del(14)(q22)	Del83775	Del 12q, del 14q	Negative	ND	*NAB2* In4/ *STAT6* In1, *NAB2* In6/ *GLI1* In1	Pos	Ex4-Ex3/ *TERT*+ C228T
21.	46,XY,der(6)t(6;13)(p21;q?32), der(13)t(6;13)(p21;q13)	ND	ND	ND	ND	ND	ND	ND/ND
22.	43–45,XY,add(6)(q21),-7,?der(11) del(11)(p13)t(?7;11)(q11;q24), −13,-14,?add(18)(q21),inc	ND	ND	ND	ND	ND	ND	ND/ND
23.	46,XX,tas(11;13)(p15;p13)	Negative	Normal	*NAB2* 5'	ND	*NAB2* In3/ *STAT6* In19	Pos	Ex4-Ex3/ *TERT*-
24.	90–92,XXYY,del(1)(p32p34)x2, der(10)t(10;?17)(q25;q21),-12,-12, −17,+der(?)t(?;12)(?;q15)x2	Split80218/83775	ND	ND	ND	ND	ND	Ex4-Ex3/ND
25.	88–90,X?,-Y,-Y,add(6)(q14),del(12) (q21)x2,+der(?)t(?;1)(?;q12)hsr(?),inc	ND	ND	*NAB2* 5'	ND	ND	ND	Ex4-Ex3/ND
26.	46,XX,der(11)t(11;12)(p11;p11) t(11;12)(q25;q13),der(12)add(12) (p1?1)add(12)(q13)	Split82324	ND	*NAB2* 5'	ND	ND	ND	Ex4-Ex3/ND
27.	46,XY,t(1;12)(p22;q13),t(9;15) (q13;q11)	Split80218	Abnormal	*NAB2* 5' *STAT6* 3'	Yes	*NAB2* In6/ *STAT6* Ex17	ND	Ex6-Ex17*/ND
28.	46,XX,t(9;12;14)(q22;q15;q23)	Split80218	ND	*NAB2* 5'	ND	ND	ND	Ex4-Ex3/ND
29.	46,XX	ND	ND	*NAB2* 5'	ND	ND	ND	Ex2-Ex3/ND
30.	46,XX	ND	ND	ND	ND	ND	ND	Ex7*-Ex18*/ ND
31.	46,XY	ND	ND	*NAB2* 5'	ND	ND	ND	Ex4-Ex3/ND
32.	46,XY,del(1)(q31q43)	Del83775	Del 12q	*NAB2* 5' *STAT6* 3'	Yes	ND	ND	Ex6-Ex17/ND
33A.	46,XX,t(4;12)(q35;q13),del(13)(q14),	Split80218/123,	Del 12q,	*NAB2* 5'	Yes	*NAB2* In4/	Pos	Ex4-Ex3/ND
33B.	add(19)(p13) 46,XX,t(4;12)(q35;q13),del(13)(q14), add(19)(p13)	Del83775–88969, Dim123 ND	del 13q Del 12q, del 13q	ND	ND	*STAT6* In1, *C12orf68* Ex1/ *NAB2* In4 ND	ND	ND/ND
34.	83–92,XXXX,ins(7;?)(p21;?)x2, del(12)(q13q14)x2,-13	ND	ND	*NAB2* 5'	ND	ND	Pos	Ex4-Ex3/ND
35.	47,XY,+der(?22)	ND	ND	Negative	ND	ND	ND	Neg/ND
36.	47,XY,+8	Negative	Del 14q	*NAB2* 5'	ND	Negative	ND	Ex4-Ex3/ND
37.	91,XXYY,-13,i(13)(q10)	ND	ND	Negative	ND	ND	ND	Ex4-Ex3/ND
38.	46,XX	ND	ND	*NAB2* 5'	ND	ND	ND	Ex4-Ex5/ND
39.	46,XX	ND	ND	*NAB2* 5'	ND	ND	ND	Ex4-Ex3/ND

TABLE 1. (Continued)

Case no.	Karyotype	FISH[a]	SNP[b]	qRT-PCR[c]	GGE[d]	NGS[e]	IHC[f]	RT-PCR/PCR[g]
40.	46,XX,add(19)(q13)	ND	ND	*NAB2* 5'	ND	ND	ND	Ex4-Ex3/ND
41.	46,XY	ND	ND	*NAB2* 5'	ND	ND	ND	Neg/ND
42.	42–46,XY,-1,add(5)(p15),-7,-8,-11, der(14)t(?10;14)(q11;p13),-15,add(17)(q25),+der(17)t(10;17)(q11;q25),-19, −20,+22,+mar,+1–2r,inc	Amp976+571	Complex gain/loss 12q, del 13q, del 14q	Negative	ND	ND	ND	Ex4-Ex3/ND
43.	48,XX,+8,der(12)	Gain83775+571	Complex gain of 12	*NAB2* 5'	ND	ND	ND	Ex4-Ex3/ND
44.	46,XX	ND	ND	*NAB2* 5'	ND	ND	ND	Neg/ND

[a]FISH, fluorescence in situ hybridization for 12q13 rearrangements. ND, not done; Negative, normal signals at metaphase FISH with BAC probes RP11–976L20 and RP11–571M6 and fosmid G248P83775F6; Del83775, loss of one signal for fosmid G248P83775F6; Split80218/83775, split signals for fosmids G248P80218G8 and G248P83775F6; Split82324, split signals for fosmid G248P82324F1; Split80218, split signals for fosmid G248P80218G8; Split80218/123, split signals for fosmid G248P80218G8 and BAC RP11–123K3; Del83775–88969, deletion of fosmids G248P83775F6, G248P84159F12, and G248P88969D9; Dim123, diminished signal for BAC RP11–123K3; Amp976+571, amplified signals for BAC probes RP11–976L20 and RP11–571M6, but not fosmid G248P83775F6, on marker chromosome; Gain83775+571, The der(12) chromosome contained two extra copies of BAC RP11–571M6 and fosmid G248P83775F6, but no copy of BAC RP11–976L20.

[b]Results of single nucleotide polymorphism (SNP) array analyses. Only data for 12q, 13q, and 14q are displayed here. For detailed results, see Supporting Information Tables S4 and S5. ND, not done; abnormal, imbalances other than loss of 12q, 13q, and/or 14q were detected.

[c]Quantitative real-time polymerase chain reaction (qRT-PCR) for the 5'- and 3'-ends of *NAB2* and *STAT6*. ND, not done; *NAB2* 5' = higher (>2 fold) expression of the 5' end than of the 3' end of *NAB2*; *STAT6* 3' = higher (>2 fold) expression of the 3' end than of the 5' end of *STAT6*; Negative, no increased expression of 5' *NAB2* or 3' *STAT6*.

[d]GGE, global gene expression analysis; ND, not done.

[e]NGS, next generation sequencing of enriched 1 Mb region in 12q13 (chr12:57,300,000–58,300,000). ND, not done. Detailed information about detected breakpoints is found in Supporting Information Table S9.

[f]IHC, immunohistochemistry on tissue microarrays for expression of GRIA2; ND, not done; pos, cytoplasmic staining for GRIA2; neg, no staining for GRIA2.

[g]Results of RT-PCR analysis for *NAB2*/*STAT6* fusion transcripts and PCR analysis for *TERT* promoter mutations. For the RT-PCR results, the exons fused to each other are indicated, using reference sequences NM_005967.3 for *NAB2* and NM_001178078.1 for *STAT6*. Asterisks (*) indicate breakpoints inside exons; fusion transcripts compatible with both intronic and exonic breakpoints were interpreted as due to intronic rearrangements. ND, not done; Neg, negative with all RT-PCR combinations. The *TERT* promoter data were published before (Killela et al., 2013). *TERT*- = negative for *TERT* promoter mutation; *TERT*+ C228T = positive for the C228T mutation in the *TERT* promoter.

Global Gene Expression Analysis

Unsupervised principal component analysis based on the expression of the 695 most variable genes ($\sigma/\sigma\max = 0.4$) showed that the five SFTs formed a group that had an expression profile separate from the control tumors (Supporting Information Fig. S1). Of the 695 most variable genes, 125 genes showed a significantly different (82 with higher and 43 with lower) expression between SFT and the control tumors ($P < 0.001$, FDR < 0.01; Supporting Information Tables S6 and S7).

When studying the expression levels of genes implicated in EGR1 signaling, we defined transcriptional deregulation as a >2-fold difference in average expression levels between the SFTs and the control tumors. Using this cut-off, 1,398 of 21,755 (6.4%) genes were either up-regulated (757 genes, 3.5%) or down-regulated (641 genes, 2.9%) in the SFTs.

We compared our global gene expression data with two data sets on EGR1 targets, which we considered of relevance for fibroblastic tumors (Supporting Information Table S8). First, Bhattacharyya et al. (2011) identified 647 genes (638 of which were present in our data set) that were differentially expressed in cultured human skin fibroblasts upon 48 hours incubation with an adenoviral recombinant containing an active *EGR1*. Second, genes with reported binding sites for EGR1 listed in the Cold Spring Harbor Laboratory Transcriptional Regulatory Element Database (CSHLTRED; http://rulai.cshl.edu/cgi-bin/TRED/tred.cgi?process=home; accessed on Nov 30, 2012) were retrieved; of a total of 102 genes, the 77 genes listed as "known" with respect to "Best promoter quality" and "Best binding quality" were included for comparison. Deregulated genes identified by us (here defined as >2-fold mean expression difference between SFTs and control tumors) were significantly over-represented among the genes identified as deregulated by forced *EGR1* expression in fibroblasts (Bhattacharyya et al., 2011): of their 638 genes, 122 (19.1%) were deregulated in our data set (122 observed vs. 41 expected, $p<0.0001$), the vast majority (100 genes, 82%) being down-regulated in the SFTs (100 observed vs. 19 expected, $p<0.0001$). Of the 77 EGR1 target genes selected from the CSHLTRED database, 14 (18.2%) showed at least 2-fold higher (five genes) or lower (nine genes) average expression levels in the SFTs than in the control tumors. Thus, genes deregulated in our array study were enriched also in this data set (14 observed vs. 5 expected; $P < 0.05$).

qRT-PCR

Tumors serving as controls had similar expression levels of the 5'- and 3'-ends of *NAB2* and *STAT6*. In contrast, an up-regulation of 5' *NAB2* was seen in 25 (71%) SFTs, in five cases together with simultaneous differential up-regulation of 3' *STAT6*; one case showed differential up-regulation only of 3' *STAT6* (Table 1, Supporting Information Figs. S2 and S3). Five of six cases showing up-regulation of 3' *STAT6* had fusion transcripts in which the *STAT6*-part started with exon 17 or 18. Of the 10 cases that were negative for differential 5' *NAB2* expression, two were negative at RT-PCR for *NAB2/STAT6* and the remaining cases had *NAB2/STAT6* fusion transcripts involving exons 2 or 4 of *NAB2* (Table 1).

Deep Sequencing of the Breakpoint Region in 12q13

The mean target coverage ranged from 485 to 867 times, with 98.2–98.3% aligned reads. A summary of identified gene fusions is provided in Table 1 and Supporting Information Tables S9 and S10, and exemplified in Supporting Information Fig. S4. In brief, fusion events were detected in 10/11 tumor samples from nine of 10 patients; the two samples from Case 1 showed identical fusions. In nine of the cases, at least one of the algorithms indicated a *NAB2/STAT6* fusion, reciprocal in three of them, at the genomic level. Genomic breakpoints mapped to intron 6 of *NAB2* in five cases, to intron 4 in two and to exon 2 or intron 3 in one case each. The genomic breakpoints in *STAT6* ranged from intron 1 to intron 19 (Supporting Information Table S9). Case 2 also showed fusions of *STAT6* to *R3HDM2* (mapping to 12q13) and *TRAPPC5* (mapping to 19p13); the latter fusion was in agreement with the cytogenetic finding of a three-way t(6;12;19). Case 20 also showed a *NAB2/GLI1* (*GLI1* is located telomeric of *NAB2* in 12q13) fusion and Case 33A had a *C12orf68/NAB2* fusion (*C12orf68* maps to the centromeric side of *NAB2* in 12q13).

RT-PCR for NAB2/STAT6 Fusion Transcripts

In-frame *NAB2/STAT6* fusion transcripts were found in 37/41 cases (Table 1). A wide distribution of breakpoints at the transcript level necessitated the use of several primer combinations. All fusion

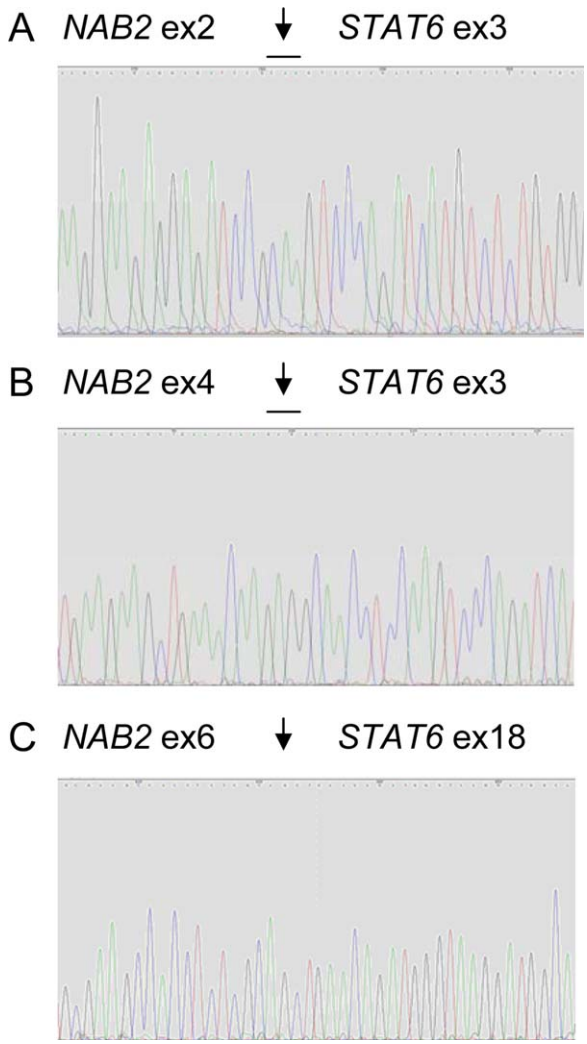

Figure 1. Chromatograms depicting three types of *NAB2/STAT6* junction in solitary fibrous tumor. Arrows indicate fusion points. A: Fusion of part of exon 2 of *NAB2* with exon 3 of *STAT6* (Case 11). The exact breakpoint cannot be identified as three nucleotides in the fusion region were shared (horizontal bar). B: Fusion sequence compatible with exonic breakpoints in both genes, but intronic breakpoints leading to fusion of the entire exon 4 of *NAB2* with the entire exon 3 of *STAT6* seem more likely (Case 20). Three shared nucleotides are indicated by horizontal bar. C: Fusion of exon 6 of *NAB2* with exon 18 of *STAT6* (Case 2). [Color figure can be viewed in the online issue, which is available at wileyonlinelibrary.com.]

transcripts contained at least the first two exons of *NAB2* and the last six exons of *STAT6*, with fusions between *NAB2* exon 4 and *STAT6* exon 3 (17 cases) and between *NAB2* exon 6 and *STAT6* exon 17 (six cases) being the most common (Table 1, Fig. 1). The majority of the fusion sequences were compatible with intronic breakpoints, but four cases had exonic breakpoints in *NAB2* and/or *STAT6*.

Immunohistochemistry

GRIA2 was the top up-regulated gene in our global gene expression series, showing very high expression values in all investigated cases. It was also found to be transcriptionally up-regulated in the studies by Hajdu et al. (2010) and Robinson et al. (2013). We thus evaluated its expression on the protein level using an antibody on a TMA previously described (Möller et al., 2011). Of nine SFTs, eight showed strong cytoplasmic staining in at least one of four cores. Only one of the 40 control tumors, a myoepithelial tumor, showed any positive staining (Supporting Information Fig. S5).

DISCUSSION

Chmielecki et al. (2013) and Robinson et al. (2013) recently showed that SFTs recurrently display fusion of two neighbouring, and partly overlapping, genes in chromosome band 12q13: *NAB2*, which is transcribed from centromere to telomere, and *STAT6*, which is transcribed from telomere to centromere. However, the results of these two studies otherwise differed significantly. Chmielecki et al. found a *NAB2/STAT6* fusion in only 29/53 (55%) cases, always with one of exons 3–7 of *NAB2* being juxtaposed with the full-length *STAT6* cDNA, and concluded that the essential outcome is deregulation of STAT6 targets (Chmielecki et al., 2013). In contrast, Robinson et al. (2013) identified a *NAB2/STAT6* fusion in all of their 51 analyzed SFTs, the most common (75%) type of fusion being between exon 6 or 7 of *NAB2* with exon 17 or 18 of *STAT6*. As all fusions detected by them would result in a chimeric protein that exchanged one or more repressor domains of NAB2 for an activation domain from STAT6, they concluded that the essential outcome was disturbed NAB2 activity, leading to deregulated early growth response (EGR) signaling. This claim was substantiated by thorough gene expression analysis and various functional in vitro studies (Robinson et al., 2013).

Our results on the *NAB2/STAT6* fusion were more in agreement with those of Robinson et al. (2013) than with those of Chmielecki et al. (2013). First, a *NAB2/STAT6* fusion transcript was found in the vast majority (37 of 41; 90%) of the cases that could be analyzed. Furthermore, in two of the four fusion-negative cases there was differential expression of the 5'-part of *NAB2*, suggesting that some SFTs might have fusion transcripts that require other primer combinations than used here. We cannot exclude poor sampling in the remaining two fusion-negative cases; in fact, one of them (Case 9) was negative also at chromosome banding, FISH and SNP array analyses, indicating few

tumor cells in the biopsy. Thus, it may well be that SFTs consistently show a *NAB2/STAT6* fusion gene. Interestingly, however, the types of fusion transcript we detected were different from those seen in the two previous studies. Like Robinson et al. (2013), we did not detect a single case in which exon 1b of *STAT6* was included in the fusion transcript, a phenomenon seen in all cases reported by Chmielecki et al. (2013). We believe that this discrepancy has a technical (RNA sequencing vs exome sequencing) rather than a biological explanation. However, the distribution of fusion breakpoints detected by us was slightly different from what was reported by Robinson et al. While they found fusions of exon 6 or 7 of *NAB2* with exon 17 or 18 of *STAT6* in 75% of their cases, such transcripts were found only in 10/37 (27%) cases in the present series (Table 1). Instead, a fusion between *NAB2* exon 4 with *STAT6* exon 3 dominated (17/37 cases; 46%) in our series; this fusion type was seen in only 3/51 (6%) cases by Robinson et al. (2013). Whether this difference is associated with phenotypic aspects, such as tumor size, location or aggressiveness will have to be evaluated in larger series.

In the present study, we used deep sequencing of an enriched 1 Mb region of 12q13 to identify at the nucleotide level the outcome of the rearrangements that had been observed by cytogenetic, FISH and SNP array analyses. The simultaneous presence of inversions, deletions and translocations in the target region made the analysis difficult at the genomic level, and all of the algorithms used had shortcomings—fusion genes are more difficult to detect at the DNA level than at the transcript level (Ozsolak and Milos, 2011). Furthermore, the capturing procedure required blocking of repeated sequences, in our case leaving out one-third of the target region, thereby potentially lowering the possibility to detect certain fusion events. Nevertheless, a *NAB2/STAT6* fusion was identified in 9/10 cases, including both samples from one of the cases, and the localization of the breakpoints at the genomic level was mostly in good agreement with the RT-PCR results; some of the discrepancies in the localization of breakpoints could be explained by splicing effects. Not unexpectedly, also other fusions were detected, e.g., between *STAT6* and *TRAPPC5* in Case 2. *TRAPPC5* maps to chromosome band 19p13, which was shown by cytogenetics to be the recipient of 12q13-material through a three-way translocation t(6;12;19)(p22;q13;p13). Another, potentially pathogenetically important fusion between intron 6 of *NAB2* and intron 1 of the *GLI1* oncogene was seen in Case 20; while RT-PCR showed a *NAB2/STAT6* fusion transcript, an additional fusion between *NAB2* and *GLI1* could not be verified at the transcript level (data not shown).

On the basis of the results of the present and previous studies we can conclude that the *NAB2/STAT6* fusion, resulting in a chimeric protein in which the carboxy-terminal repressor domain of NAB2 is replaced with a highly variable portion of STAT6, is a primary and presumably pathogenetic event in SFT development. Furthermore, our results and those by Robinson et al. (2013) convincingly show that irrespective of anatomic site of origin and morphologic subtype (i.e., absence/presence of malignant features, prominent branching vessels or fat), SFTs share the same genetic origin.

The origin of the fusions is likely due to simultaneous inter- and intrachromosomal rearrangements, as shown here by cytogenetics, FISH and deep sequencing at the DNA level. As *NAB2* and *STAT6* are located close to each other, but transcribed in different orientations, a fusion event requires an inversion. Furthermore, SNP array analysis revealed frequent 12q deletions with centromeric breakpoints within or immediately downstream of *STAT6*, and banding analysis showed translocations of chromosome arm 12q with various other chromosomes. Because the level of genetic instability seems to be low (identical karyotypes and SNP array profiles in the primary lesion and, five years later, in the relapse from Case 33), we believe that the *NAB2/STAT6* fusion results from a single, complex rearrangement involving multiple chromosomal breakpoints.

We also agree with Robinson et al. (2013) that the cellular effects of the *NAB2/STAT6* fusion could be attributed to distorted NAB2 activity. The *NAB2* gene consists of 7 exons, encoding a 525 aa protein. Two conserved domains—NCD1 and NCD2—are encoded by exon 2 and exons 2–3, respectively (Svaren et al., 1997); NCD1 is essential for interaction with EGR1, while NCD2 is important for transcriptional repression. Also the carboxy-terminal part (amino acids 386–525, corresponding to exons 5–7) is important for transcriptional repression, containing a chromodomain helicase DNA-binding protein 4 (CHD4)-interacting domain (CID); deletion of exon 6 (amino acids 426–489) creates a CHD4-independent form of NAB2 (Srinivasan et al., 2006). As NAB2 interacts with EGR1, and the EGR1-interacting NCD1 domain is always present in the fusion protein,

one would expect to find an enrichment of EGR1 target genes among the genes that were differentially expressed in SFTs. Indeed, such an association was shown by Robinson et al. (2013), as well as in this study (Supporting Information Table S8).

EGR1, the most extensively analyzed of four EGR proteins, is a zinc finger DNA-binding transcription factor, the expression of which is induced by a variety of stimuli, including ultraviolet light, hormones, cytokines, and growth factors such as TGF-β. Aberrant function of EGR1 has been implicated in many disease-associated processes, such as cancer, inflammation, fibrosis, and epithelial-mesenchymal transition (Bhattacharyya et al., 2011, 2013). One of the target genes of EGR1 is *NAB2*, showing increased expression levels soon after the induction of *EGR1* transcription (Svaren et al., 1996, 1997, 1998; Srinivasan et al., 2006; Bhattacharyya et al., 2008). NAB2, in turn, regulates the expression of EGR1 target genes by binding, on the one hand, to the R1 inhibitory domain of EGR1 and, on the other, to the CHD3 and CHD4 proteins (Srinivasan et al., 2006). CHD3 and CHD4 are enzymatic subunits of the nucleosome remodeling and histone deacetylase (NuRD) complex, a key regulator of gene expression at the chromatin level (Lai and Wade, 2011). The NuRD multi-protein complex consists of subunits with enzymatic activity (CHD3 and CHD4 and histone deacetylases HDAC1 and HDAC2) and of non-enzymatic subunits (methyl-CpG-binding domain proteins MBD2 and MBD3, metastasis-associated proteins MTA1, MTA2, MTA3, and retinoblastoma-binding proteins RBBP4 and RBBP7 (Lai and Wade, 2011). The NuRD complex regulates gene transcription through at least two mechanisms: deacetylation of histones and nonhistone proteins and ATP-dependent chromatin remodeling resulting in repositioning of nucleosomes (Lai and Wade, 2011; Allen et al., 2013). It is currently not known how the NuRD complex is attracted to a given promoter, but some transcriptional co-factors, including NAB2, that bind NuRD have been identified. Of the genes encoding members of the NuRD complex, all showed the same expression levels in SFTs and control tumors, except the *CHD3* gene which showed a 2-fold higher expression among SFTs (data not shown).

When we compared our global gene expression data with two data sets on EGR1 targets (Bhattacharyya et al., 2011 and the CSHLTRED database), we found that genes showing deregulated expression (here defined as >2-fold mean expression difference between SFTs and control tumors) at global gene expression analysis were enriched among EGR1 target genes (Supporting Information Table S8). Possibly reflecting the fact that Bhattacharyya et al. used a NAB-resistant *EGR1* construct, our down-regulated genes were equally common among their up-regulated (62/370, 16.8%) and down-regulated (38/268, 14.2%) genes. An interesting aspect of our gene expression data was that the majority of the presumed EGR1 target genes were found to be transcriptionally down-regulated in SFTs. As wt NAB2 acts as a repressor of EGR1 activity, the NAB2/STAT6 chimera, which lacks carboxy-terminal parts that are considered important for repression, could be expected to augment transcription of EGR1 targets. Indeed, Robinson et al. (2013) demonstrated an increased expression of an EGR1 reporter in an in vitro assay when comparing the effects of NAB2/STAT6 with wt NAB2. Possibly, our finding of mostly down-regulated EGR1 targets could be partly explained by the choice of EGR1 target genes in the present study. It should be kept in mind, however, that the effects of EGR1 are still poorly characterized, and NAB2 can sometimes potentiate rather than repress EGR1-dependent transcription; thus, to categorize NAB2 as a transcriptional repressor is probably an over-simplification (Bhattacharyya et al., 2008). In addition, the potential impact of the carboxy-terminal part of STAT6 on the NAB2/STAT6 chimera and its interaction with EGR1 and other proteins must also be considered. The exact effects of the NAB2/STAT6 fusion protein will have to be investigated in functional assays.

Also several genes of importance in fetal development showed differential expression, suggesting that the pathogenetic mechanism in SFT involves epigenetic deregulation of multiple down-stream target genes. Of 38 *HOX* genes for which data were available (*HOXC4* not included in our data), 20 showed 2.0–6.9-fold higher average expression values in SFTs than among the controls (Supporting Information Table S11). None of the *HOXD* genes showed this phenomenon. These results are in agreement with Robinson et al. (2013), who also identified increased expression of *HOXB* and *HOXC* genes. Furthermore, it was recently shown that the NuRD complex is vital for normal differentiation of embryonic stem cells, at least in part by down-regulating the expression of the *ZFP42*, *TBX3*, *KLF4*, and *KLF5* genes. Deletion of the *MBD3* gene, encoding a scaffold protein that is

essential for the assembly of the NuRD complex, leads to up-regulation of these genes, thereby blocking differentiation (Reynolds et al., 2012). Intriguingly, *TBX3* and *KLF4* expression was reduced more than 2-fold in the SFTs, and *ZFP42* showed very low expression levels in all tumor types. Combined with the finding of widespread *HOX* gene up-regulation, these findings suggest a fundamental disturbance of developmentally important genes in SFTs.

The top up-regulated gene in our series was *GRIA2*; the average expression level was more than 100 times higher than in the control tumors (Supporting Information Table S6). A similar overexpression was seen in the studies by Hajdu et al. (2010) and Robinson et al. (2013). *GRIA2* encodes a subunit of a class of glutamate receptors that are involved in a variety of neurophysiological processes, including transmission of excitatory synaptic signals. The GRIA2 protein is normally not detected outside the CNS, but aberrant expression has been detected in various malignancies. We have no explanation to why *GRIA2* shows such a high expression in SFTs, but it could be noticed that one important regulator of *GRIA2* is the transcription factor nuclear respiratory factor 1 (NRF1), the DNA-binding activity of which is influenced by post-translational acetylation. Furthermore, GRIA2 is a main target for the REST corepressor complex, which includes HDAC1 and HDAC2 (Noh et al., 2012). Regardless of the underlying mechanism, the strongly increased expression suggests that the GRIA2 protein might be of diagnostic interest. Currently, CD34 is the standard discriminator at IHC, but CD34 is not expressed in all SFTs and several other soft tissue tumors are also CD34-positive (Fletcher et al., 2013b). To explore whether the increased mRNA expression translates into increased expression also at the protein level, we performed IHC analysis with a GRIA2-specific antibody on a TMA previously described (Möller et al., 2011). The analysis showed expression of GRIA2 in 8/9 SFTs but only in one of the control tumors (a myoepithelial tumor), warranting further IHC studies of SFTs and morphologically similar tumors (Supporting Information Fig. S5).

The clinical outcome for patients with SFT is difficult to predict at diagnosis. Some factors that are known to be associated with increased risk of relapse include a high mitotic count, location outside the trunk wall or extremities, and large tumor size (Fletcher et al., 2013a). The *NAB2/STAT6* fusion as such is unlikely to be of prognostic relevance as it is present regardless of tumor location, histopathologic subtype and malignancy grade. Furthermore, we could not discern any correlation between type of fusion transcript and any of these parameters in the present study. Bearing in mind that the genetic background of the *NAB2/STAT6* fusion varied considerably, e.g., ploidy levels ranged from hypodiploid to tetraploid, and that certain chromosomal rearrangements, notably losses of 13q and 14q, were recurrent, we compared the genomic profiles of 11 "aggressive" tumors (tumors that were diagnosed as malignant and/or metastasized) with those of 33 benign tumors. However, no clinicogenetic associations were found (data not shown). Interestingly, two of 10 SFTs (Cases 17 and 20) had mutations in the *TERT* promoter (Table 1). Apart from the presence of 14q-deletions at cytogenetic analysis in both cases, there was nothing that set the *TERT*-positive cases apart from the negative ones. *TERT* promoter mutations were recently shown to be highly frequent among myxoid liposarcomas, but otherwise rare (frequency less than 1%) in benign and malignant bone and soft tissue tumors (Killela et al., 2013). Whether the relatively high frequency of *TERT* mutations in SFTs is associated with cell of origin or the nature of the fusion gene is presently unknown.

In conclusion, we confirm that *NAB2/STAT6* fusions are common in SFTs, and we agree with Robinson et al. (2013) that the essential outcome is disturbed function of NAB2, rather than deregulation of STAT6. Combining what is known about the function of NAB2, the nature of the *NAB2* rearrangements detected and global gene expression data on SFTs, the pathogenetic basis of SFT is a deregulated interaction between NAB2, EGR1 and the NuRD complex. In turn, this results in widespread disturbances in gene regulation, particularly prominent for genes involved in the EGR-signaling pathway. However, also genes not previously directly implicated in EGR-signaling, such as the *HOX* genes and genes involved in stem cell plasticity, show deregulated expression in SFTs, suggesting that much could be learnt about the function of NAB2 by studying SFTs. The finding of NAB2 as a key player in SFT pathogenesis might also explain why previous attempts to use targeted treatments have failed to result in anything but very limited effects on the outcome. Previously selected targets, such as the VEGF pathway, IGF2 signaling, or tyrosine kinases are all, at best, secondary mediators of the underlying genetic aberration. For instance, the

finding that tyrosine kinase inhibitors like sunitinib could provide a partial response could perhaps be explained by EGR1 being regulated by ABL1 (Bhattacharyya et al., 2011). Similarly, the previous focus on IGF2 and IGF2 signaling is unlikely to yield any dramatic therapeutic effects, as this is only one of several pathways affected by the disturbed gene expression pattern.

ACKNOWLEDGMENTS

The authors acknowledge the help with SNP array analyses from the Swegen Centre for Integrative Biology at Lund University.

REFERENCES

Allen HF, Wade PA, Kutateladze TG. The NuRD architecture. Cell Mol Life Sci (in press). DOI 10.1007/s00018-012-1256-2.

Bertucci F, Bouvier-Labit C, Finetti P, Adélaïde J, Metellus P, Mokhtari K, Decouvelaere AV, Miguel C, Jouvet A, Figarella-Branger D, Pedeutour F, Chaffanet M, Birnbaum D. 2013. Comprehensive genome characterization of solitary fibrous tumors using high-resolution array-based comparative genomic hybridization. Genes Chromosomes Cancer 52:156–164.

Bhattacharyya S, Wei J, Melichian DS, Milbrandt J, Takehara K, Varga J. 2008. The transcriptional cofactor Nab2 is induced by TGF-β and suppresses fibroblast activation: physiological roles and impaired expression in scleroderma. PLoS One 4:e7620.

Bhattacharyya S, Wu M, Fang F, Tourtellotte W, Feghali-Bostwick C, Varga J. 2011. Early growth response transcription factors : Key mediators of fibrosis and novel targets for anti-fibrotic therapy. Matrix Biol 30:235–242.

Bhattacharyya S, Fang F, Tourtellotte W, Varga J. 2013. Egr-1: New conductor for the tissue repair orchestra directs harmony (regeneration) or cacophony (fibrosis). J Pathol 229:286–297.

Chmielecki J, Crago AM, Rosenberg M, O'Connor R, Walker SR, Ambrogio L, Auclair D, McKenna A, Heinrich MC, Frank DA, Meyerson M. 2013. Whole-exome sequencing identifies a recurrent *NAB2-STAT6* fusion in solitary fibrous tumors. Nat Genet 45:131–132.

Demicco EG, Park MS, Araujo DM, Fox PS, Bassett RL, Pollock RE, Lazar AJ, Wang W-L. 2012. Solitary fibrous tumor: A clinicopathological study of 110 cases and proposed risk assessment model. Mod Pathol 25:1298–1306.

DePristo MA, Banks E, Poplin RE, Garimella KV, Maguire JR, Hartl C, Philippakis AA, del Angel G, Rivas MA, Hanna M, McKenna A, Fennell TJ, Kernytsky AM, Sivachenko AY, Cibulskis K, Gabriel SB, Altshuler D, Daly MJ. 2011. A framework for variation discovery and genotyping using next-generation DNA sequencing data. Nat Genet 43:491–498.

Fletcher CDM, Bridge JA, Lee J-C. 2013a. Extrapleural solitary fibrous tumour. In: Fletcher CDM, Bridge JA, Hogendoorn PCW, Mertens F (Eds.) World Health Organization Classification of Tumours. Pathology and Genetics of Tumours of Soft Tissue and Bone. Lyon: IARC Press, pp. 80–82.

Fletcher CDM, Bridge JA, Hogendoorn PCW, Mertens F, editors. 2013b. World Health Organization Classification of Tumours. Pathology and Genetics of Tumours of Soft Tissue and Bone. Lyon: IARC Press.

Ge H, Liu K, Juan T, Fang F, Newman M, Hoeck W. 2011. FusionMap: detecting fusion genes from next-generation sequencing data at base-pair resolution. Bioinformatics 27:1922–1928.

Guillou L, Fletcher JA, Fletcher CDM, Mandahl N. 2002. Extrapleural solitary fibrous tumour and haemangiopericytoma. In: Fletcher CDM, Unni KK, Mertens F, editors. World Health Organization Classification of Tumours. Pathology and Genetics of Tumours of Soft Tissue and Bone. Lyon: IARC Press, pp. 86–90.

Hajdu M, Singer S, Maki RG, Schwartz GK, Keohan ML, Antonescu CR. 2010. IGF2 overexpression in solitary fibrous tumors is independent of anatomic location and is related to loss of imprinting. J Pathol 221:300–307.

Jin Y, Möller E, Nord KH, Mandahl N, Vult Von Steyern F, Domanski HA, Mariño-Enríquez A, Magnusson L, Nilsson J, Sciot R, Fletcher CDM, Debiec-Rychter M, Mertens F. 2012. Fusion of the *AHRR* and *NCOA2* genes through a recurrent translocation t(5;8)(p15;q13) in soft tissue angiofibroma results in upregulation of aryl hydrocarbon receptor target genes. Genes Chromosomes Cancer 51:510–520.

Killela PJ, Reitman ZJ, Jiao Y, Bettegowda C, Agrawal N, Diaz LA Jr, Friedman AH, Friedman H, Gallia GL, Giovanella BC, Grollman AP, He T-C, He Y, Hruban RH, Jallo GI, Mandahl N, Meeker AK, Mertens F, Netto GJ, Rasheed BA, Riggins GJ, Rosenquist TA, Schiffman M, Shih I-M, Theodorescu D, Torbenson MS, Velculescu VE, Wang T-L, Wentzensen N, Wood LD, Zhang M, McLendon RE, Bigner DD, Kinzler KW, Vogelstein B, Papadopoulos N, Yan H. 2013. *TERT* promoter mutations occur frequently in gliomas and a subset of tumors derived from cells with low rates of self-renewal. Proc Natl Acad Sci USA 110:6021–6026.

Klemperer P, Rabin CB. 1931. Primary neoplasm of the pleura: A report of five cases. Arch Pathol 11:385.

Lai AY, Wade PA. 2011. Cancer biology and NuRD: A multifaceted chromatin remodelling complex. Nat Rev Cancer 11:588–596.

Li H, Durbin R. 2009. Fast and accurate short read alignment with Burrows-Wheeler transform. Bioinformatics 25:1754–1760.

Li H, Handsaker B, Wysoker A, Fennell T, Ruan J, Homer N, Marth G, Abecasis G, Durbin R, 1000 Genome Project Data Processing Subgroup. 2009. The sequence alignment/map format and SAMtools. Bioinformatics 25:2078–2079.

Livak KJ, Schmittgen TD. 2001. Analysis of relative gene expression data using real-time quantitative PCR and the $2^{-\Delta\Delta C_T}$ method. Methods 25:402–408.

Mandahl N, Heim S, Arheden K, Rydholm A, Willén H, Mitelman F. 1988. Three major cytogenetic subgroups can be identified among chromosomally abnormal solitary lipomas. Hum Genet 79:203–208.

Miettinen MM, el-Rifai W, Sarlomo-Rikala M, Andersson LC, Knuutila S. 1997. Tumor size-related DNA copy number changes occur in solitary fibrous tumors but not in hemangiopericytomas. Mod Pathol 10:1194–1200.

Mitelman Database of Chromosome Aberrations and Gene Fusions in Cancer 2013. Mitelman F, Johansson B, Mertens F, editors. Available at: http://cgap.nci.nih.gov/Chromosomes/Mitelman.

Möller E, Hornick JL, Magnusson L, Veerla S, Domanski HA, Mertens F. 2011. *FUS-CREB3L2/L1* positive sarcomas show a specific gene expression profile with upregulation of *CD24* and *FOXL1*. Clin Cancer Res 17:2646–2656.

Noh K-M, Hwang J-Y, Follenzi A, Athanasiadou R, Miyawaki T, Greally JM, Bennett MVL, Zukin RS. 2012. Repressor element-1 silencing transcription factor (REST)-dependent epigenetic remodeling is critical to ischemia-induced neuronal death. Proc Natl Acad Sci USA 109:E962–E971.

Ozsolak F, Milos PM. 2011. RNA sequencing: Advances, challenges and opportunities. Nat Rev Genet 12:87–98.

Panagopoulos I, Mertens F, Domanski HA, Isaksson M, Brosjö O, Gustafson P, Mandahl N. 2001. No *EWS/FLI1* fusion transcripts in giant cell tumors of bone. Int J Cancer 93:769–772.

Rausch T, Zichner T, Schlattl A, Stütz AM, Benes V, Korbel JO. 2012. DELLY: structural variant discovery by integrated paired-end and split-read analysis. Bioinformatics 28:i333–i339.

Reynolds N, Latos P, Hynes-Allen A, Loos R, Leaford D, O'Shaughnessy A, Mosaku O, Signolet J, Brennecke P, Kalkan T, Costello I, Humphreys P, Mansfield W, Nakagawa K, Strouboulis J, Behrens A, Bertone P, Hendrich B. 2012. NuRD suppresses pluripotency gene expression to promote transcriptional heterogeneity and lineage commitment. Cell Stem Cell 10:583–594.

Robinson DR, Wu Y-M, Kalyana-Sundaram S, Cao X, Lonigro RJ, Sung Y-S, Chen C-L, Zhang L, Wang R, Su F, Iyer MK, Roychowdhury S, Siddiqui J, Pienta KJ, Kunju LP, Talpaz M, Mosquera JM, Singer S, Schuetze SM, Antonescu CR, Chinnaiyan AM. 2013. Identification of recurrent *NAB2-STAT6* gene fusions in solitary fibrous tumor by integrative sequencing. Nat Genet 45:180–185.

Shaffer LG, Slovak ML, Campbell LJ. 2009. An International System for Human Cytogenetic Nomenclature (2009). Basel: Karger.

Srinivasan R, Mager GM, Ward RM, Mayer J, Svaren J. 2006. NAB2 represses transcription by interacting with the CHD4 subunit of the nucleosome remodeling and deacetylase (NuRD) complex. J Biol Chem 281:15129–15137.

Svaren J, Sevetson BR, Apel ED, Zimonjic DB, Popescu NC, Milbrandt J. 1996. NAB2, a corepressor pf NGFI-A (Egr-1) and Krox20, is induced by proliferative and differentiative stimuli. Mol Cell Biol 16:3545–3553.

Svaren J, Apel ED, Simburger KS, Jenkins NA, Gilbert DJ, Copeland NA, Milbrandt J. 1997. The *Nab2* and *Stat6* genes share a common transcription termination region. Genomics 41: 33–39.

Svaren J, Sevetson BR, Golda T, Stanton JJ, Swirnoff AH, Milbrandt J. 1998. Novel mutants of NAB corepressors enhance activation by Egr transactivators. EMBO J 17:6010–6019.

Vallat-Decouvelaere AV, Dry SM, Fletcher CDM. 1998. Atypical and malignant solitary fibrous tumors in extrathoracic locations: Evidence of their comparibility to intra-thoracic tumors. Am J Surg Pathol 22:1501–1511.

Weiss SW, Goldblum JR. 2008. Soft Tissue Tumors, 5th ed. Mosby Elsevier: Philadelphia.

Ye K, Schulz MH, Long Q, Apweiler R, Ning Z. 2009. Pindel: A pattern growth approach to detect break points of large deletions and medium sized insertions from paired-end short reads. Bioinformatics 25:2865–2871.